Potential Core Lengths of Round Jets in Stagnant and Moving Environments

C. M. Or[1], K. M. Lam[2] and P. Liu[1]

[1]Graduate Student, [2]Associate Professor,

Department of Civil Engineering, The University of Hong Kong, Pokfulam Road,

Hong Kong, China

Corresponding author: Dr. K. M. Lam

Department of Civil Engineering, The University of Hong Kong,

Pokfulam Road, Hong Kong, China

Tel: (852) 2859 1975

Fax: (852) 2559 5337

E-mail: kmlam@hku.hk

Potential Core Lengths of Round Jets in Stagnant and Moving Environments

C. M. Or, K. M. Lam and P. Liu

Abstract: This paper investigates the change of velocity and concentration fields in the initial region of a round jet in stagnant fluid and in a moving environment of the co-flow, counter-flow or cross-flow situation. The aim was to discuss issues of flow establishment and in the initial region, to determine the potential core length, and to observe the effect of a moving ambient. Turbulent jet velocities and concentration were measured with the planar imaging techniques of particle image velocimetry (PIV) and laser-induced fluorescence (LIF). The mean flow fields were obtained and analyzed to investigate the validity of $1/x$ decay relationship for jet centerline velocity and concentration. Values for the decay constant and jet virtual origin were obtained from the data. While the results show that the decay constant is increased by a co-flow but reduced by a counter-flow or a cross-flow, the virtual origin was found to be affected as well. The overall effect is that any situation of the moving environment leads to a slight reduction of the physical length of the potential core. The paper also suggests an intermittency function for the analysis of fluctuating jet concentration field in the potential core. The mean intermittency function provides a direct and reliable estimate of the potential core length of a jet in a moving environment.

1. Introduction

A submerged round jet is often used for the purpose of wastewater discharge into water bodies such as rivers and oceans due to its rapid mixing and dilution capability. The presence of an ambient flow usually enhances mixing and dilution of the jet. It is thus important to understand the mixing behaviour of a jet submerged in stagnant and moving environments. The mostly studied moving ambient cases include the co-flow, cross-flow and counter-flow situations. While there have been many studies aiming at the measurement or prediction of jet behaviour in those moving environments and in stagnant ambient (Fischer et al. 1979, Wood et al. 1993, Jirka 2004, for review), most of them investigated

the "far field" of the jet, or the zone of established flow (ZEF). In the ZEF, self similarity behaviour is observed on the spreading of the jet as measured by various mean flow properties including the growth of jet width, the decay of jet centreline properties with axial distance, and the radial profiles of velocity and concentration. This self similarity of jet behaviour in the ZEF have facilitated the development of integral models for the prediction of jet dilution (e.g., Jirka 2004).

At the jet exit, jet effluent is discharged in the form of a core of fluid with constant exit velocity (and effluent concentration) leading to strong shear with the ambient fluid. The jet shear layer then grows and starts to erode the "potential core" from outside towards the jet centerline. This initial region of jet development is termed the zone of flow establishment (ZFE) where the initial top-hat type profiles of mean velocity and mean concentration transits to the final similarity profiles at the ZEF (e.g., Abramovich 1963). The flow transition from ZFE to ZEF is complex and gradual but the changes are mostly completed within an axial distance of about 5 to 10 jet-exit-diameters, D (e.g., Antoine et al. 2001). In hydraulic applications where the interests are mostly on the mixing and dilution efficiency at large distances from the jet exit, the ZFE or the potential core has not been given much attention. This may explain why most integral models do not distinguish between the ZFE and the ZEF. In these models, calculations start from the jet exit and the effect of the ZFE is taken into account by some adjusted initial conditions.

The ZFE is important in governing the initial development of the jet, especially the case for a jet in a moving environment. The length of the ZFE or the potential core may also affect the prediction of far field dilution. For instance, the far field trajectory of a jet in a cross-flow eventually runs along the direction of the cross-flow but the offset distance from the jet exit can be affected significantly by the length of the ZFE. There are also observations suggesting that improved integral model predictions in the initial region of the jet (e.g., within the first $15D$) can be achieved through an explicit treatment of the ZFE length from which the computation starts (e.g., Kwan 1998).

Another issue in the near field behaviour of a jet is the jet virtual origin, the point from which the self-similar behaviours in the ZEF of the jet are projected to start. The virtual origin is often neglected in hydraulic applications but it may be located from the physical jet exit at a distance of as much as $5D$ (Antoine et al. 2001).

In this investigation, turbulent velocity and concentration fields were measured in the initial $15D$ region of round jets in a number of stagnant and moving environments including

the co-flow, cross-flow and counter-flow situations. The data were analyzed to study the decay of jet centerline properties in the ZEF and the length of the ZFE with the effect of the jet virtual origin. Then, a method of direct determination of the potential core length using flow data inside the ZFE was proposed. Afterwards, the effect of a moving environment on the potential core length was discussed.

2. Experiments

Laboratory experiments were conducted in a 1.2 m wide partition of the 12 m × 5 m shallow water basin in the Croucher Laboratory of Environmental Hydraulics at the University of Hong Kong. Water was set at 1 depth in the basin. A circular nozzle with exit diameter $D = 10$ mm was placed at mid-depth to discharge water in the form of a horizontal submerged round jet. The jet effluent was supplied from an overhead tank at a constant head. To have a turbulent jet condition, the jet exit velocity, U_j, was set at a value between 0.36 m/s and 0.37 m/s. The Reynolds number was Re $= U_j D/\upsilon \approx 4,000$. Experiments and measurements were carried out with the round jet in stagnant water and in a number of ambient flow situations, which included the co-flow, cross-flow and counter-flow situations. The moving environment condition was simulated by towing the jet in the basin of stagnant water at a constant speed U_o. The towing system consisted of a platform on trolleys and was powered by a step motor with speed controlled by a computer. A co-flow and counter-flow ambient was created by towing the jet along the jet exit direction, while a cross-flow ambient was created by towing a horizontally rotated jet in the basin. This technique has been reported in Lam et al. (2006) and a schematic diagram of the present set up is shown in Fig. 1. In each ambient flow situation, different strengths of the ambient current were tested with the jet-to-current velocity ratio, $R = U_j/U_o$, varied from 2 to 20.

Time-varying velocity and concentration fields in the initial region of the jet were measured with the techniques of particle-image velocimetry (PIV) and laser-induced fluorescence (LIF), respectively. In this study, these planar flow diagnostic techniques made non-intrusive velocity and concentration measurements on the horizontal longitudinal plane of the jet flow field. For PIV measurements, the jet effluent and water in the basin were seeded with neutrally buoyant particles of 30-micron nominal diameter. A double-pulsed Nd:YAG laser was used to illuminate the flow on the measurement plane through a window on the

side of the water basin. A PIV camera was mounted on the platform together with the jet nozzle and was thus towed together with the jet. To avoid image distortion due to surface waves, a hollow glass tank was placed touching the water surface and towed together with the camera (Fig. 1). The firing rate of the pulses was 10 Hz, which means that the temporal resolution was 10 PIV snapshots per second. For each flow case, about 1000 snapshots were captured to ensure reliable statistical estimate of the stationary turbulent jet flow. At fast values of U_o, the 1000 snapshots could not be obtained within one tow and a number of tows were made to capture the required number of snapshots for reliable measurement of time-averaged mean flow behavior.

The double-pulsed PIV images were analyzed by a PIV analysis software (Dantec Dynamic Studio) which was based on the spatial cross-correlation algorithm of Willert and Gharib (1991) but with adaptive and multi-pass interrogation windows. All velocity vectors were validated with a threshold of signal-to-noise ratio at about 1.2 for the correlation peaks. Rejected vectors were replaced by vectors estimated from the surrounding values. In the final iteration, PIV vectors are obtained on interrogation areas of size 32 pixels $\times$ 32 pixels and with 50% overlap. With the camera resolution at 1344 pixels $\times$ 1024 pixels, the two-dimensional velocity field at each time instant consisted of 83 $\times$ 63 vectors of U and V. In most tests, this spatial extent of the PIV measurements was about $8.6D \times 6.5D$ and the spatial resolution of the velocity vectors was thus approximately $0.1D$.

In some flow cases, the same optical set up for PIV was used for concentration measurement with LIF. Fluorescent dye Rhodamine 6G was added to the jet effluent at a constant concentration and an orange filter was added in front of the camera to pass only the fluorescent light signal. Only one of the dual images from the PIV camera was used for LIF analysis from which concentration levels were computed from the gray levels. In other flow cases, LIF measurements were made with a continuous wave Argon-ion laser for illumination and a high-speed camera for image capture. Those LIF measurements covered a larger measurement region area up to about $15D$ in length.

3. Potential core length from velocity and concentration changes in ZEF

3.1. Decay of jet velocities in simple jet

In many past studies, the length of the ZFE is indirectly determined from the decay of centerline velocity or concentration in the ZEF. For a round jet in stagnant ambient, that is, the "simple jet", many previous studies (e.g., Fischer et al. 1979) found that the centerline velocity or concentration decays with $-1/x$ in the self-preserving ZEF as:

$$\frac{U_c}{U_j} = \frac{K_1}{(x - x_0)/D} = \frac{L - x_0}{x - x_0} \tag{1}$$

where x is the axial distance from the (physical) jet exit, U_c is the jet centerline velocity and L is the length of ZFE (from the physical jet exit). When projected upstream, the x^{-1} decay (and the linear growth of jet width) is traced back to start at the virtual origin of the jet which is located at $x = x_0$, and with K_1 being the decay constant (Hussein et al. 1994, Antoine et al. 2001). Ignoring the virtual origin, the ZFE length is usually assigned the value $K_1 D$. For velocity, the commonly accepted value for K_1 is 6.2 (Fischer et al. 1979) but the review in Antoine et al. (2001) of past studies of the simple jet and jets in very weak coflow suggests that the value of K_1 can occupy a wide range between 5.8 and 6.7.

The importance of the virtual origin is often overlooked in many studies but Antoine et al. (2001) reviewed that x_0 can be as large as $5D$. This may significantly affect the indirectly determined value of the physical ZFE length whose actual distance from the jet exit is found from Eq. (1) as:

$$L = K_1 D + x_0 \tag{2}$$

While it is a common assumption that the virtual origin is located downstream of the physical jet exit, that is $x_0 > 0$, there are experimental data indicating negative values for x_0 (Antoine et al. 2001, Uddin and Pollard 2007).

For the simple jet at Re = 4,130, Fig. 2 shows the mean velocity vectors from PIV measurements. They show the global spreading behaviour of the simple jet, such as decay of mean jet centerline velocity and growth of jet width along downstream direction. In addition, the transition from ZFE to ZEF can also be identified from the development of radial velocity profiles (as shown by the envelopes of the vectors at successive axial locations). Following the procedures in many past studies, the development of centerline velocity is plotted in Fig. 3(a) in the form of U_j/U_c against x/D in order to determine the values of K_1 and x_0 in Eq. (1). It is observed that a linear curve can be fitted to the data for $x/D > 3$. The fitting gives a negative value of x_0 at $-2.4D$ and a decay constant at $K_1 = 5.1$. This value of K_1 is lower than the range of variation reported in previous studies. The decay constant of a turbulent round jet can vary over a range of values depending on factors

including initial velocity profiles, nozzle shapes, and amount of flow entrainment near jet exit (Antoine et al. 2001, Xu and Antonia 2002, Babu and Mahesh 2004, Quinn 2006). The negative value of x_0 implies that the virtual origin is located upstream of the jet exit and the physical length of the potential core from the jet exit is shorter than $K_1 D$ (Fig. 2). The length of the potential core, measured from the jet exit, has the value $L = (5.1-2.4)D = 2.7D$.

3.2. Jet velocity decay of jets in co-flow and counter-flow

The mean velocity field of a jet in co-flow is similar to that of a simple jet except that the jet velocities would approach the co-flow velocity at sufficiently long distances downstream (Xia and Lam 2009). Fig. 4 shows two examples of the mean velocity fields of a jet in co-flow at velocity ratio $R = 10$ and 2.5. The mean spreading behaviour of a round jet in a counter-flow has been reported in Lam and Chan (1997, 2002). Fig. 5 shows the mean velocity vectors of a jet in a weak and a strong counter-flow. The results at the strongest counter-flow under test, $R = 2.5$, shows the typical flow pattern of a jet in counter-flow where jet penetration and backward turning can be observed. At a weaker counter-flow, for instance, in Fig. 5(a), the jet penetrates through a long distance and the data up to $x/D = 8$ cannot show the end of the penetration. Many studies showed that the penetration distance, x_p, of a round jet in a counter-flow varies linearly with the velocity ratio. Saghravani and Ramamurthy (2010) recently confirmed that the relationship $x_p/D \approx 2.7R$ applies to unconfined jet in a counter-flow. This is consistent with the result in Fig. 5(b).

The decay curves of jets in co-flow and counter-flow have been plotted in Fig. 3(b). It is clearly observed that presence of a counter-flow significantly increases the rate of decay. The effect of a co-flow is not as obvious but comparing to the simple jet, the centerline velocity starts to decay at a farther upstream location in the presence of a co-flow.

For a jet in co-flow, Fig. 6 shows examples of plot of U_j/U_c against x/D at $R = 20$ (the weakest co-flow) and at $R = 2.5$ (the strongest co-flow). In the present measurement region, the jet centerline velocities still follow the x^{-1} decay. At large x where the jet velocities become insignificant comparing to the co-flow, the decay will change to $x^{-2/3}$ (Fischer et al. 1979). From the best straight line fit to the data of $U_j/U_c(x)$ in Fig. 6, the values of K_1 and x_0 are obtained and their values have large differences between the two velocity ratios. Table 1 lists the values of K_1 and x_0 at all five velocity ratios under study. The physical lengths of ZFE from the jet exit as calculated from Eq. (2) are also listed. In all cases, negative values

are found for x_0. In the weaker co-flows, the decay constant has values within a narrow range at K_1 between 5.5 and 5.9. Large differences in values are found when the co-flow becomes stronger at $R \leq 5$.

The effect of a co-flow in reducing the decay rate of $U_c(x)$ was supported previously (e.g., Chu et al. 1999) by the argument of a smaller shear velocity around the jet exit expected in the presence of a co-flow. The present results in Table 1 show that K_1 increases from the simple jet value as the co-flow becomes stronger (that is, decreasing values of R). However, the results also show that in a stronger co-flow, x_0 becomes more negative, that is, the virtual origin is shifted towards the upstream of the jet exit. The overall result is that the value of L remains essentially constant at $2D$ to $2.3D$ in all co-flow cases, except in the strongest tested co-flow, at $R = 2.5$, where $L = 1.5D$. A similar qualitative observation can also be made from the centerline velocity decay curves in Fig. 3. A plot of the data in Table 1 is given in Fig.7. A recent study also suggests that the physical length of the ZFE is decreased by the presence of a co-flow (Xia and Lam 2009).

For a jet in counter-flow, Fig. 3(b) already shows that the ZFE length is shortened and the jet centerline velocity decays at a much faster rate. The curves of $U_j/U_c(x)$ at $R = 2.5$ and $R = 10$ are shown in Fig. 8. In the weaker counter-flow ($R = 10$), the jet behaves very similar to the simple jet in the initial region (Fig. 5(a)). Fig. 8 shows that the jet centerline velocity at $x/D < 6$ follows the x^{-1} decay to which Eq. (1) can be fitted. In the stronger counter-flow at $R = 2.5$, the jet penetrates through an axial distance to about $7D$ only (Lam and Chan 1997, 2002; Saghravani and Ramamurthy 2010). However, the data in Fig. 8 suggests that the x^{-1} jet centerline velocity decay seems still valid at the initial part of the jet penetration distance. It is obvious that the data of U_j/U_c within the first few diameter distance from x/D = 2.5 follow a linear trend and Eq. (1) can be fitted to those data. . The fitted values of K_1 and x_0 for all cases of jet in counter-flow are presented in Table 1 and Fig. 7. As expected, the decay constant K_1 clearly becomes smaller (that is, a faster decay rate) as the counter-flow becomes stronger. However, the change in values of x_0 follows an opposite trend, that is x_0 having a higher value with a stronger counter-flow. Thus, the resulting values of L lie within a narrow range between $2.0D$ and $2.4D$ over all the counter-flow velocity ratios.

3.3. Jet velocities of jets in cross-flow

In a cross-flow, the jet bends towards the cross-flow direction. In a weak cross-flow, the bending is not significant in the initial region, say, $x/D < 14$ for $R = 20$ in Fig. 9(a). The jet centerline trajectory, shown superimposed on the mean velocity vectors in Fig. 9, is obtained by tracking the locations of maximum mean axial velocity, $U_c = \max(U)$ at successive x-sections of the jet. The change of these "centerline" mean axial velocities with x is shown in Fig. 10. The $1/x$ decay of U_c applies only within a short distance downstream of the potential core at $x/D < 6$. An attempt is made to fit Eq. (1) to the data within these axial distances and the values of K_1 and x_0 are obtained as shown in the figure.

At $R = 6$, the jet trajectory is bent to more than 45° in Fig. 9(b). Comparing to Fig. 9(a), the jet exit velocity decays quickly and a potential core of constant jet velocities cannot be readily revealed by the mean vector plot. For the mean axial velocities along the jet trajectory, shown in Fig. 10, the $1/x$ decay can only be fitted over a very short distance between $x/D = 2$ and 4.

It is evident from the PIV results that the ZFE of a jet in cross-flow cannot be confidently deduced by the change of jet properties in the relatively far field. Nevertheless, an attempt is made to fit the $1/x$ decay to the change of jet centerline velocity over the short distance just downstream of the potential core. The values of K_1 and x_0 so obtained are listed in Table 2 for the different velocity ratios of the cross-flow. As expected, when the cross-flow changes from weak to strong (that is, decreasing values of R), the decay constant K_1 becomes monotonically smaller, that is, the jet centerline velocity decays faster. However, the jet virtual origin is also changed by R. The combined result on the potential core length is that L remains fairly constant at about $2D$ in a cross-flow weaker than $R \geq 4$ but when the cross-flow is stronger, L becomes significantly shorter.

3.4. Change of effluent concentration in ZEF

While the velocity field provides information on the mixing and spreading of the jet, measurement of concentration field of jet effluent can directly reveal the dilution of a jet. In this study, time varying concentration fields in each flow case was obtained from the LIF images. Some examples of mean concentration field $C(x, y)$ are shown as gray-level images in Fig. 11 which includes jets in a co-flow (a), a counter-flow (b) and a cross-flow (c). In the co-flow at $R = 10$, the jet spreads similar to the simple jet. The counter-flow at $R = 4$ increases the spreading of the jet and turns the jet backwards at $x/D \approx 11$. The cross-flow at

9

$R = 6$ bends the jet in the lateral direction but no significant bending effect on the potential core is observed.

In the gray-level images of concentration field in Fig. 11, the potential core is revealed as the bright conical region attached to the jet exit where the tracer concentration is the highest. This potential core or ZFE for the concentration field has a different length from that for the velocity field. Previous studies suggested that the length of this ZFE applicable to the tracer concentration field, L_T, is shorter than the ZFE length of the velocity field (e.g., Xia and Lam 2009). For the simple jet, it is commonly accepted that the centerline concentration remains unchanged at the jet exit concentration inside L_T and then decays with x^{-1} in the ZEF:

$$\frac{C_c}{C_j} = \frac{K_T}{(x - x_0)/D} = \frac{L_T - x_0}{x - x_0} \tag{3}$$

Here, C_c is the centerline concentration, C_j is the scalar concentration at jet exit and K_T is the decay constant of centerline concentration. The decay constant is often quoted to have a value at $K_T = 5.0$ (e.g., Fischer et al. 1979) while Antoine et al. (2001) suggested values between 5.1 and 6.3. The virtual origin, x_0, may also be different from that of the velocity field.

Similar to the velocity field, the potential core length for concentration may be determined indirectly from a fitting to Eq. (3) of centerline concentration data in the ZEF of the simple jet or, in the case of jet in a current, within the region downstream of the potential core where the x^{-1} decay is observed. For brevity, the data fitting in this study is not shown but the resulting values of K_T, x_0, and L_T for some jet cases are summarized in Table 3. For the simple jet, the decay constant has an average value of $K_T = 5.8$ from a number of test runs. The virtual origin for the decay of effluent concentration is found to be upstream of the jet exit, having a value of $x_0 = -2.1D$. For the simple jet, the variation of the values of L_T, from $L_T = K_TD + x_0$, is smaller than that of K_T or x_0 among all test runs. The average value of potential core length is $3.7D$.

For a jet in counter-flow, the x^{-1} decay of centerline concentration is observed only within the first part of the penetration distance (similar to the observation in Fig. 8). It is found that both K_T and L_T remains essentially constant at $R > 5$ but showing a slightly decreasing trend with decreasing values of R, that is with a stronger counter-flow (Table 3). At $R < 5$, the potential core length is remarkably reduced by the counter-flow.

For the jets in co-flow, it is interesting to observe from Table 3 that the variation of the decay rate, as reflected by the value of K_T, is limited to about 10% only. The location of jet virtual origin shows a larger variation over the different strengths of co-flow. The resulting potential core length is found to be reduced slightly by the co-flow, from $L_T/D = 2.60$ at $R = 20$ to $L_T/D = 1.82$ at $R = 2.5$. It is commonly accepted that under a co-flow, a jet spreads with a slower rate (e.g., Chu et al. 1999). This is not readily observed in the present data of K_T. In Fig. 13, the mean concentration field is shown in the form of axial development of radial concentration profiles for jet in a weak co-flow at $R = 10$ and jet in a strong co-flow at $R = 2.5$. The jet widths, as found from the locations of concentration level drops to $1/e$ times the centerline value, are plotted superimposed on the profiles. Comparing the slope of the jet width curves shows that the jet widths in the strong co-flow are smaller than those in the weak co-flow at the same downstream distances.

4. Direct determination of potential core length

4.1. Analysis of concentration field in ZFE

It is shown in the previous section that the indirect method of inferring the potential core length from the velocity or concentration data in the downstream region may incur difficulties, especially for a jet in counter-flow or cross-flow. The planar LIF technique enables time histories of concentration to be obtained on the whole (x, y) plane and not just along the centerline. It is thus possible to directly determine the location of the potential core from the concentration data in the initial region. A number of techniques have been proposed by the present authors (Or et al. 2007) and the more reliable ones are briefly described here using the example of LIF results of a jet in a co-flow at $R = 10$.

After long time averaging, the mean concentration field of the round jet in a co-flow at $R = 10$ is obtained as already shown in Fig. 11(a). The potential core can be qualitatively observed from the gray-level image of $C(x, y)$ but a quantitative determination of its exact length is required. The change of mean concentration along the jet centerline is shown in Fig. 13. The transition from ZFE to ZEF is not as ideal as Eq. (3) which dictates that C_c remains constant at C_j inside the potential core and suddenly follows the x^{-1} decay downstream of $x = L_T$. The potential core length L_T, found by fitting Eq. (3) to the data in

ZEF, is the x location where the x^{-1} decay curve meets the $C_c = C_j$ line. In a moving environment where the centerline concentration does not follow the x^{-1} decay, the potential core length cannot be confidently determined from the decay of $C_c(x)$ downstream of the potential core. Provided that the jet exit concentration is obtained precisely, a simple method of directly measuring the potential core length is to track the x location where the centerline concentration drops to, say, 0.9 or some other fractions of the exit level. However, the choice of the fraction is up to debate.

In jets and mixing layers, the intermittency function has been used to describe quantitatively turbulence mixing of one fluid such as the potential core jet fluid with the other fluid such as the ambient environment (e.g., Andreopoulos 1985). It was originally applied to turbulent velocity signals measured by the hot wire or turbulent temperature signals. Davidson and Wang (2002) extended the application to time history of jet concentration field. Or et al. (2007) suggested that the intermittency function can be used to find the location of the potential core since inside the ZFE, the potential core contains jet effluent at the exit concentration and the concentration should remain constant with time given no mixing with the ambient environment. The intermittency function is defined as the amount of "non-intermittency" of the concentration signal due to turbulent dilution of the ambient fluid. It should have a value of unity or 100% inside the potential core. Outside the potential core, turbulent mixing with the surrounding fluid takes place and the concentration level is decreased due to dilution. The intermittency function thus drops below unity.

In this paper, the time-dependent intermittency function, $I(x, y, t)$, at a point is calculated from the comparison of instantaneous concentration at that point with the initial exit concentration C_j. As an illustration, Fig. 14(a) shows the example of one instantaneous concentration field in the initial region of a jet. The corresponding region of unity intermittency obtained from a binarization analysis is shown in Fig. 14(b) and this shows clearly the region of potential core fluid not yet diluted by mixing with the ambient fluid. From the time series of 1000 LIF images, a time series of intermittency function is obtained. The mean intermittency factor is then obtained as $I(x, y)$ in Fig. 14(c). The advantage of using this mean intermittency factor over the mean concentration field, in Fig. 11(c), in the determination of potential core length is that the drop of values is much sharper on leaving the potential core. This is illustrated by the comparison of centerline decay of $I(x, 0)$ and $C_c(x)$ in Fig. 13. For this case of a jet in a co-flow at $R = 10$, the distances at which the mean intermittency function falls to 0.9, 0.5 and 0.1 are $1.80D$, $3.06D$ and $4.50D$.

In addition to the mean intermittency function, Or et al. (2007) also proposed to carry out proper orthogonal decomposition (POD) analysis to the time series of $I(x, y, t)$ for a better estimate of the potential core length. Applications of the snapshot POD method to the concentration field of jet flow have been reported in Sirovich et al. (1990), Bernero and Fiedler (2000), Xia and Lam (2005). After POD analysis of the intermittency function, it was found that the first four modes already contain about 70% of the total energy of the fluctuations and that mode 1 alone contributes about 65%. Mode 1 describes the most dominant pattern of fluctuations and it has very similar pattern as the mean intermittency function. It was concluded in Or et al. (2007) that a confident estimate of the potential core length of a jet in a moving environment can be obtained as the x location where the mean intermittency function or the mode 1 intermittency function drops to 0.5. In this paper, the LIF data are analyzed with this technique of intermittency and direct determination of the potential core length is made from the mean intermittency function.

4.2. Potential core length of round jet in moving environment

The preceding sections describe how an estimate of the potential core length can be obtained from an ensemble of LIF concentration fields with the analysis of intermittency function. Fig. 15 shows those estimates for jets in a co-flow, counter-flow or cross-flow. In all conditions of the moving ambient, the potential core length L_T is found to be shortened with increasing strengths of the ambient current. At $R > 10$, all strengths of the weak ambient current lead to very similar values of L_T but as the ambient current becomes stronger from $R < 10$, the potential core length is shortened sharply. Similar values of potential core lengths are found between a jet in a co-flow and that in a counter-flow of the same velocity ratio, while, in comparison, a jet in a cross-flow has a shorter L_T. The values of L_T as obtained from the fitting of x^{-1} decay of jet centerline concentration (or, of sectional maximum concentration for jet in cross-flow) in the initial region of the ZEF are also shown in Fig. 15. Those values are generally lower than the directly estimated values by half to one jet-exit-diameter length.

For the ZFE length of a jet in cross-flow, Pratte and Baines (1967) proposed the following expression for L based on the velocity field:

$$\frac{L}{D} = 5.4 - 2.7e^{-0.625R} - 2.7e^{-0.041R} \tag{4}$$

In this study, the potential core length of concentration field of the simple jet is found at $L_T \approx 3.8D$. Thus, for comparison to the present data, Eq. (4) is adjusted by assuming a constant ratio between L_T and L at $L_T/L = 3.8/5.4$. The resulting curve of L_T/D is included in Fig. 15. It is observed that the curve predicts well the data at $R \leq 5$.

5. Conclusions

This paper discusses the issues and problems relating to the determination of potential core length in a round jet discharging into stagnant and moving environments. The establishment of jet flow as shown by the measurements of velocity and concentration fields in the potential core and the initial region does not support the simplified division of the jet into the ZFE and ZEF. There are unresolved issues including the significance of the virtual origin, the axial range of validity of x^{-1} decay of jet centerline velocities or concentration in a moving ambient, and the gradual change from jet exit velocity and concentration to the decaying quantities near the end of the potential core. For the concentration field, this paper proposes a direct method to measure the potential core length using the concept of intermittency function.

Experiments are carried out for jets in stagnant and moving environments where time histories of jet velocity fields and concentration fields are measured with the planar imaging techniques of PIV and LIF. In a short and selected region just downstream of the potential core, the jet centerline velocities or concentration can be fitted to the x^{-1} decay from which the decay constant and jet virtual origin are estimated. In this study, the virtual origin is often found upstream of the jet exit and this results in a short physical potential core length (as measured from the physical jet exit) which is shorter than $4D$ in most cases. This may be particular to the jet nozzle used in the study but an important and perhaps more universal observation is that the presence of an ambient moving environment changes not only the decay constant but also x_0. While the results generally support a slower decay of jet velocity or concentration in a co-flow or and a faster decay of jet in a counter-flow or in a cross-flow, the physical length of the potential core appears to be affected by the ambient current in a much lesser degree. It is found that only in a strong moving environment that the potential core is notably shortened no matter this is a co-flow, counter-flow or cross-flow situation.

The paper continues to propose a direct method to determine the potential core length from the time history of concentration field obtained in the ZFE itself. This method is based on the intermittency function which distinguishes the instantaneous potential core region of pure jet fluid. The time-varying intermittency function is obtained from the binarization of the instantaneous LIF image with the exit concentration level as the threshold. The x location at which the time-averaged mean intermittency function drops to 0.5 along the jet centerline trajectory is suggested as a reliable estimate of the physical length of the potential core. This method works well for jets in a moving environment of any situation and similarly, the resulting potential core length is found to be shortened by a counter-flow, cross-flow or co-flow at $R < 10$.

Acknowledgement

References

Abramovich, G.N. (1963). The Theory of Turbulent Jets. MIT Press, Cambridge, MA.

Andreopoulos, J. (1985). On the structure of jets in crossflow. J. Fluid Mech. 157, 163-197.

Antoine, Y., Lemoine, F., and Lebouche, M. (2001). Turbulent transport of a passive scalar in a round jet discharging into a coflowing stream. Euro. J. Mech. B/Fluids 20, 275-301.

Babu, P.C., and Mahesh, K. (2004). Upstream entrainment in numerical simulations of spatially evolving round jets. Phys. Fluids 16(10), 3699-3705.

Bernero, S., and Fiedler, H.E. (2000). Application of particle image velocimetry and proper orthogonal decomposition to the study of a jet in a counterflow. Exp. Fluids 29, S274-281.

Chu, P.C.K., Lee, J.H.W., and Chu, V.H. (1999). Spreading of turbulent round jet in coflow. J. Hydraul. Eng. 125(2), 193-204.

Davidson, M. J., and Wang, H. J. (2002). Strongly advected jet in a coflow. J. Hydraul. Eng., 128(8), 742-752.

Fischer, H.B., List, E.J., Koh, R.C.Y., Imberger, J., and Brooks, N.H. (1979). Mixing in Inland and Coastal Waters. Academic Press, New York.

Hussein, H.J., Capp, S.P., and George, W.K. (1994). Velocity measurements in a high-Reynolds-number, momentum-conserving, axisymmetric, turbulent jet. J. Fluid Mech. 258, 31-75.

Jirka, G.H. (2004). Integral model for turbulent buoyant jets in unbounded stratified flows. Part 1: The single round jet. Env. Fluid Mech. 4, 1-56.

Kwan, S.H. (1998). A study of the near-field characteristics of round turbulent jets discharged into waves. Ph.D. Thesis, Imperial College of Science and Technology, London.

Lam, K.M., and Chan, C.H.C. (2002). Time-averaged mixing behaviour of circular jet in counterflow – Velocity and concentration measurements. J. Hydraul. Eng. 128(9), 861-865.

Lam, K.M., and Chan, H.C. (1997). Round jet in ambient counterflowing stream. J. Hydraul. Eng. 123(10), 895-903.

Lam, K.M., Lee, W.Y., Chan, C.H.C. and Lee, J.H.W. (2006). Global behaviors of a round buoyant jet in a counterflow. J. Hydraul. Eng. 132(6), 589-604.

Or, C.M., Lam, K.M., and Poon, C.K. (2007). Flow establishment of concentration field in submerged round jets. Proc. 32nd IAHR Congress, Venice, July 2007, Paper 899, 1-10.

Pratte, B.D. and Baines, W.D. (1967). Profiles of the round turbulent jet in a crossflow. J. Hydr. Div., ASCE, 100, 69-83.

Quinn, W.R. (2006). Upstream nozzle shaping effects on near field flow in round turbulent free jets. Euro. J. Mech. B/Fluids 25, 279-301.

Sirovich, L., Kirby, M., and Winter, M. (1990). An eigenfunction approach to large scale transitional structures in jet flow. Phys. Fluids A 2(2), 127-136.

Saghravani, S.F. and Ramamurthy, A.S. (2010). Penetration length of confined counter flowing free jet. J. Hydraul. Eng. 136(3), 179-182.

Sirovich, L., Kirby, M., and Winter, M. (1990). An eigenfunction approach to large scale transitional structures in jet flow. Phys. Fluids A 2(2), 127-136.

Uddin, M., and Pollard, A. (2007). Self-similarity of coflowing jets: The virtual origin. Phys. Fluids, 19, 068103, 1-4.

Willert, C.E., and Gharib, M. (1991) "Digital particle image velocimetry." Exp. Fluids 10, 181-193.

Wood I.R., Bell, B.G., and Wilkinson, D.L. (1993). Ocean Disposal of Wasterwater. Advanced series in ocean engineering, Vol. 8. World Scientific, River Edge, N.J.

Xia, L.P., and Lam, K.M. (2005). Characteristics of concentration field in the initial region of a jet in coflow. Proc. 31st IAHR Congress, Seoul, September 2005, 14-26.

Xia, L.P., and Lam, K.M. (2009). Velocity and concentration measurements in initial region of submerged round jets in stagnant environment and in coflow. J. Hydro-envir. Res. 3, 21-24.

Xu, G., and Antonia, R.A. (2002). Effect of different initial conditions on a turbulent round free jet. Exp. Fluids 33, 677-683.

Nomenclature

The following symbols and abbreviations are used in this paper:

υ	kinematic viscosity
C	concentration of jet effluent
C_c	centerline concentration of jet effluent
C_j	concentration of jet effluent at jet exit
D	jet exit diameter
I	intermittency function
K_1	decay constant for jet centreline velocity
K_T	decay constant for jet centreline concentration
L	length of ZFE of jet velocity field, from physical jet exit
L_T	length of ZFE of jet concentration field
R	jet-to-current velocity ratio: $R = U_j/U_o$
Re	Reynolds number
U	axial velocity component, along x direction
U_c	jet centerline velocity
U_j	jet exit velocity
U_o	ambient flow speed of moving environment
x	axial distance from physical jet exit, along initial jet discharge direction
x_0	x location of jet virtual origin
x_p	axial distance of jet penetration of jet in counter-flow
y	lateral coordinate, perpendicular to initial jet discharge direction
ZEF	Zone of established flow
ZFE	Zone of flow establishment

Tables

Table 1

Decay constant, virtual origin and potential core length inferred from $1/x$ decay of jet centerline velocity in ZEF. Jet in co-flow or counter-flow.

Velocity ratio, R	Co-flow			Counter-flow		
	K_1	x_0/D	L/D	K_1	x_0/D	L/D
2.5	9.30	−7.79	1.51	2.03	−0.03	2.00
5	6.24	−4.17	2.07	2.15	0.14	2.29
7.5	5.87	−3.70	2.17	2.66	−0.34	2.32
10	5.65	−3.52	2.13	3.66	−1.50	2.16
20	5.47	−3.16	2.31	4.14	−1.78	2.36
(Simple jet)	(5.11)	(−2.40)	(2.71)	(5.11)	(−2.40)	(2.71)

Table 2

Decay constant, virtual origin and potential core length inferred from $1/x$ decay of jet centerline velocity in ZEF. Jet in cross-flow.

	Cross-flow		
Velocity ratio, R	K_1	x_0/D	L/D
2	0.74	0.67	1.31
4	0.99	0.43	1.42
6	1.14	0.82	1.96
8	1.77	0.10	1.86
12	3.06	−1.00	2.06
20	3.20	−1.21	1.99

Table 3

Decay constant, virtual origin and potential core length inferred from $1/x$ decay of jet centerline concentration in ZEF.

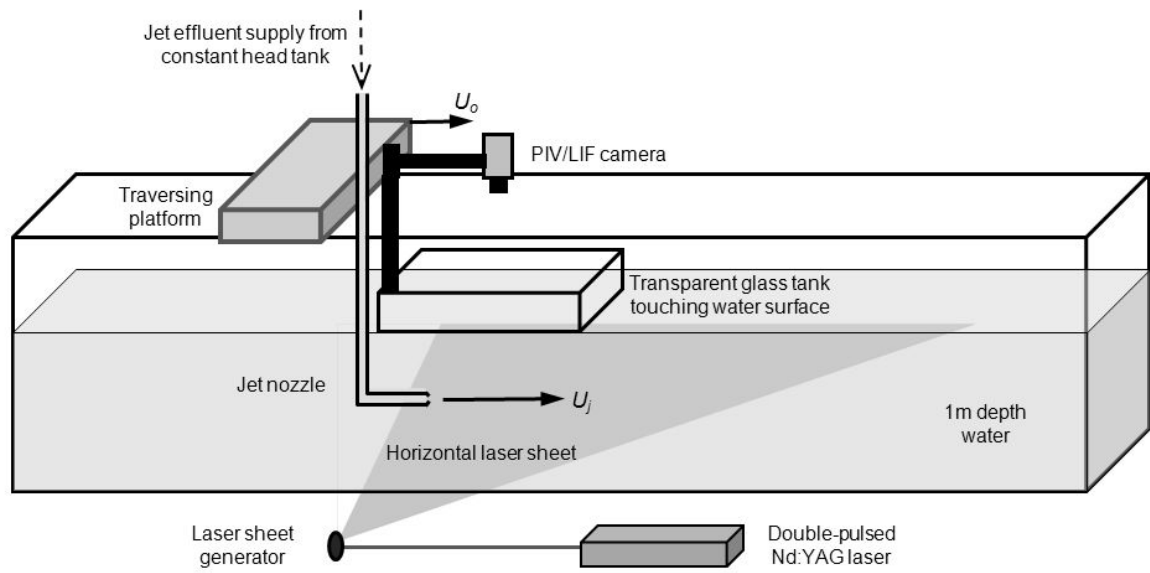| Velocity ratio, R	Co-flow			Counter-flow			Cross-flow		
	K_T	x_0/D	L_T/D	K_T	x_0/D	L_T/D	K_T	x_0/D	L_T/D
2.5	3.54	−1.72	1.82	5.65	−3.98	1.67	1.25	0.11	1.36
5	3.67	−1.30	2.38	8.11	−6.01	2.09	1.95	−0.06	1.89
10	3.75	−1.22	2.53	9.79	−7.53	2.26	4.74	−2.57	2.17
15	3.91	−1.35	2.57	9.27	−6.96	2.31	5.22	−3.02	2.20
20	4.07	−1.48	2.60	8.99	−6.56	2.42	5.65	−3.52	2.12
(Simple jet)				(5.83)	(−2.13)	(3.70)			

Figure Captions

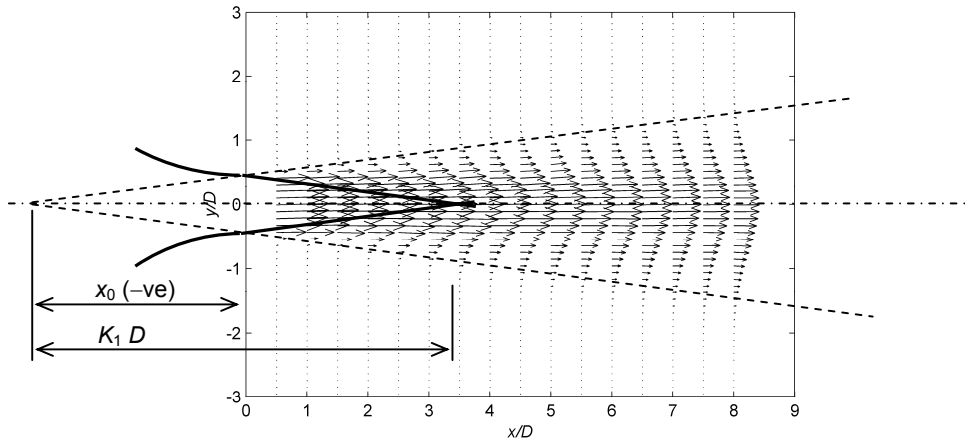Fig. 1.   Schematic diagram of experimental setup for jet in counter-flow.

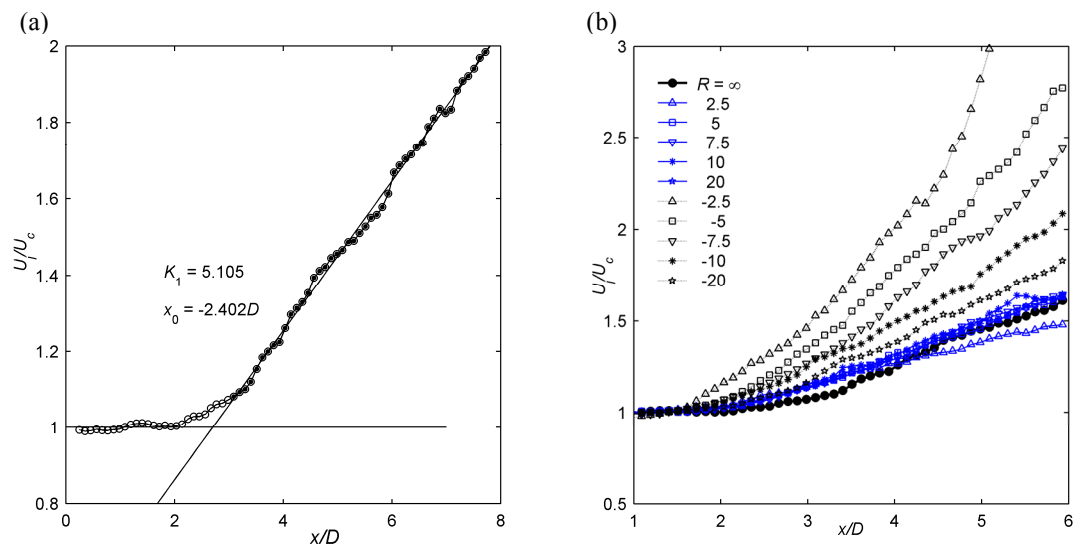Fig. 2.   Mean velocity field of simple jet at Re = 4130, with illustration of virtual origin.

Fig. 3.   Axial development of jet centerline velocity. (a) Simple jet data and fitted x^{-1} decay of Eq. (1): solid symbols showing data used in fitting. (b) Jets in co-flow and counter-flow (with negative R), and simple jet ($R = \infty$).

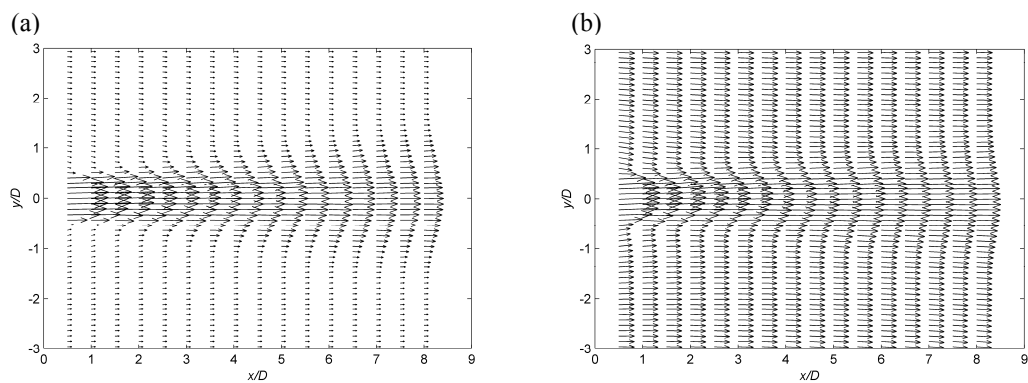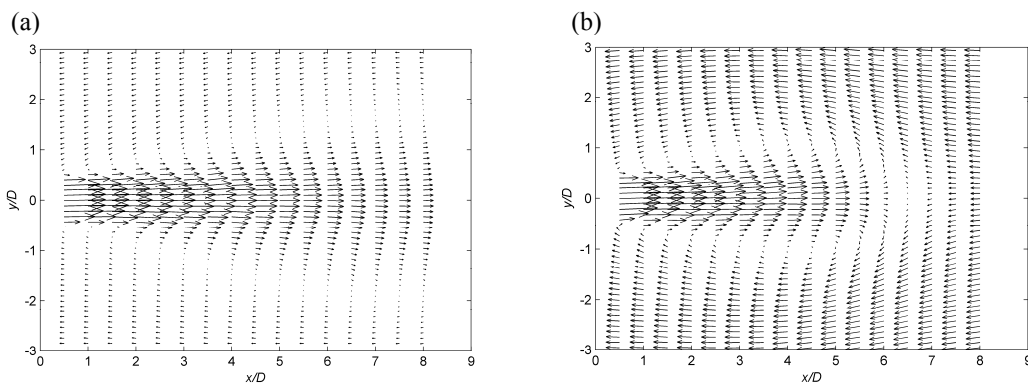Fig. 4.   Mean velocity vectors of jet in co-flow: (a) $R = 10$ (b) $R = 2.5$.

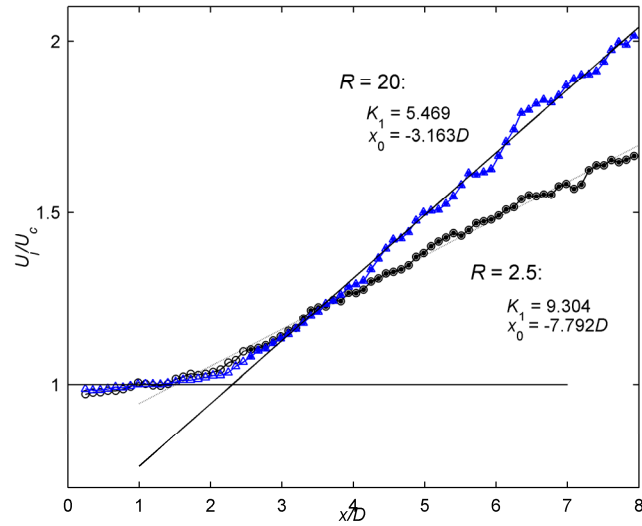Fig. 5.   Mean velocity vectors of jet in counter-flow: (a) $R = 10$ (b) $R = 2.5$.

Fig. 6.   Curves of U_j/U_c against x/D of jet in weak or strong co-flow. Solid symbols showing data used in fitting to Eq. (1).
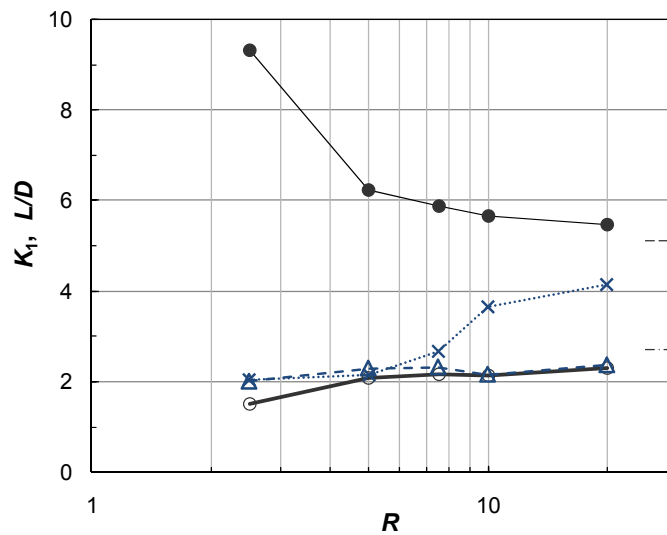
Fig. 7.   Effect of ambient current on jet parameters of K_1 and L/D. ●, ×: K_1 for jet in co-flow and counter-flow, respectively. o, Δ: L/D for jet in co-flow and counter-flow, respectively. Values of simple jet shown in far right.

Fig. 8.   Curves of U_j/U_c against x/D of jet in weak and strong counter-flow. Solid symbols showing data used in fitting to Eq. (1).

Fig. 9.   Mean velocity vectors of jet in cross-flow: (a) $R = 20$ (b) $R = 6$. Locations of sectional maximum axial velocity shown with fitted jet centerline trajectory.

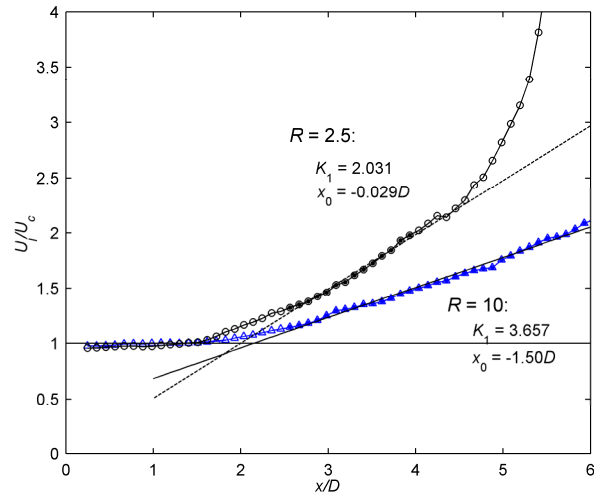Fig. 10. Curves of U_j/U_c against x/D of jet in cross-flow. Solid symbols showing data used in fitting to Eq. (1).

Fig. 11. Mean concentration field of jet shown as gray-level image. (a) in co-flow at $R = 10$ (b) in counter-flow at $R = 4$ (c) in cross-flow at R 6.

Fig. 12. Development of radial mean concentration profiles.

Fig. 13. Centerline decay of mean concentration (open symbols) and mean intermittency function (closed symbols). Jet in co-flow at $R = 10$.

Fig. 14. Potential core of jet in co-flow at $R = 10$. (a) Instantaneous concentration field, (b) instantaneous region of unity intermittency corresponding to (a) (c) gray-level field of mean intermittency function.

Fig. 15. Effect of ambient current on potential core length for concentration in jet. Symbols: $\bullet$: co-flow $\times$: counter-flow $\blacktriangle$: cross-flow. Solid lines and filled symbols: L_T determined from direct method; broken lines and open symbols: L_T determined indirectly from Eq. (3). Dotted curve: Eq. (4) adjusted to $L_T/D = 3.8$ at $R = \infty$.

Fig. 1. Schematic diagram of experimental setup for jet in counter-flow.

Fig. 2. Mean velocity field of simple jet at Re = 4130, with illustration of virtual origin.

(a)

(b)

$K_1 = 5.105$

$x_0 = -2.402D$

Fig. 3. Axial development of jet centerline velocity. (a) Simple jet data and fitted x^{-1} decay of Eq. (1): solid symbols showing data used in fitting. (b) Jets in co-flow and counter-flow (with negative R), and simple jet ($R = \infty$).

Fig. 4. Mean velocity vectors of jet in co-flow: (a) *R* = 10; (b) *R* = 2.5.

Fig. 5. Mean velocity vectors of jet in counter-flow: (a) *R* = 10; (b) *R* = 2.5.

Fig. 6. Curves of U_j/U_c against x/D of jet in weak or strong co-flow. Solid symbols showing data used in fitting to Eq. (1).

Fig. 7. Effect of ambient current on jet parameters of K_1 and L/D.
●, ×: K_1 for jet in co-flow and counter-flow, respectively.
o, Δ: L/D for jet in co-flow and counter-flow, respectively.
Values of simple jet shown in far right.

Fig. 8. Curves of U_j/U_c against x/D of jet in weak and strong counter-flow. Solid symbols showing data used in fitting to Eq. (1).

Fig. 9. Mean velocity vectors of jet in cross-flow: (a) $R = 20$; (b) $R = 6$. Locations of sectional maximum axial velocity shown with fitted jet centerline trajectory.

Fig. 10. Curves of U_j/U_c against x/D of jet in cross-flow. Solid symbols showing data used in fitting to Eq. (1).
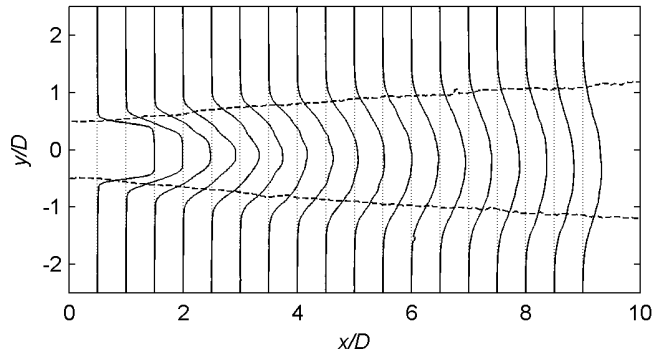
(a)

(b)

(c)

Fig. 11. Mean concentration field of jet shown as gray-level image.
(a) in co-flow at $R = 10$; (b) in counter-flow at $R = 4$; (c) in cross-flow at $R = 6$.

(a) *R* = 2.5

(b) *R* = 10

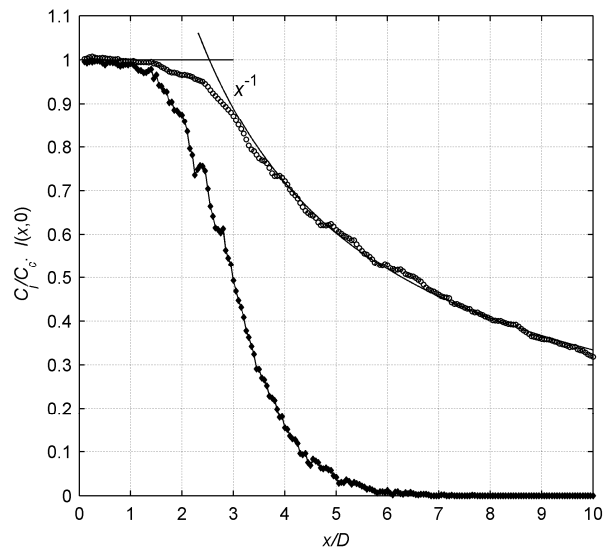Fig. 12. Development of radial mean concentration profiles.

Fig. 13. Centerline decay of mean concentration (open symbols) and mean intermittency function (closed symbols). Jet in co-flow at $R = 10$.
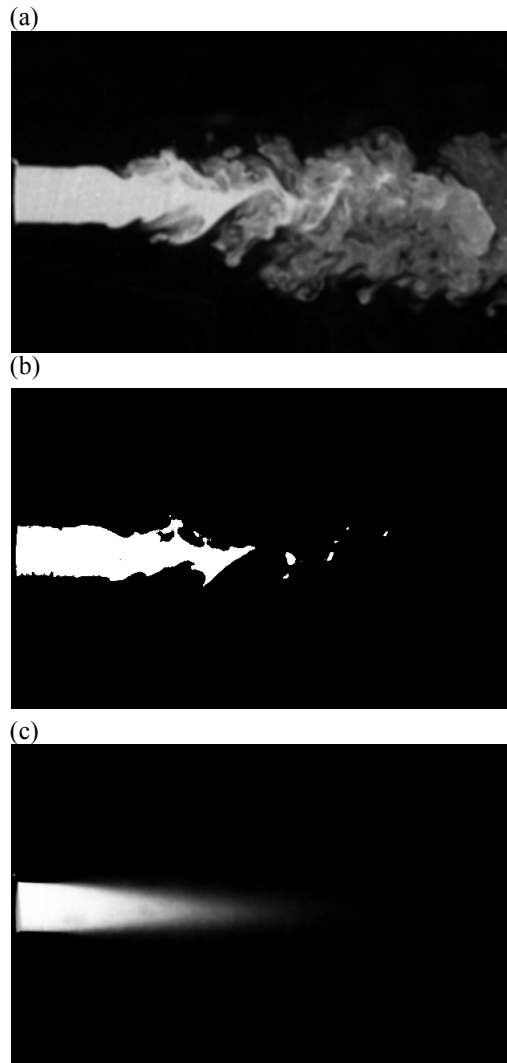
Fig. 14. Potential core of jet in co-flow at $R = 10$. (a) Instantaneous concentration field, (b) instantaneous region of unity intermittency corresponding to (a); (c) gray-level field of mean intermittency function.
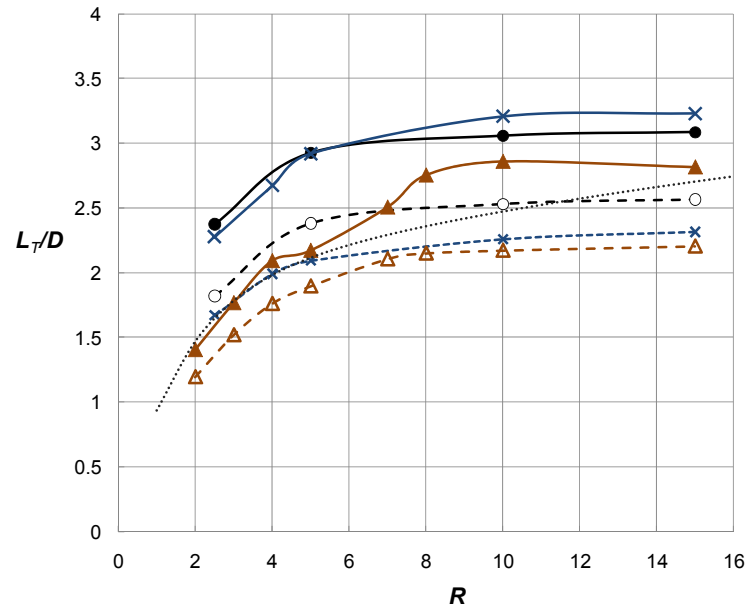
Fig. 15. Effect of ambient current on potential core length for concentration in jet. Symbols:
•: co-flow; ×: counter-flow; ▲: cross-flow. Solid lines and filled symbols: L_T determined
from direct method; broken lines and open symbols: L_T determined indirectly from Eq. (3).
Dotted curve: Eq. (4) adjusted to $L_T/D = 3.8$ at $R = \infty$.